Time-resolved $K\alpha$ spectra in high-intensity laser-target interaction

N. H. Burnett, G. D. Enright, A. Avery, A. Loen, and J. C. Kieffer*
National Research Council of Canada, Division of Physics,
Ottawa, Ontario K1A 0R6, Canada
(Received 27 September 1983)

The spectrum of $K\alpha$ emission lines resulting from the interaction of a 10-μm laser at 3×10^{14} W/cm^2 with aluminum and titanium targets has been temporally resolved with an x-ray streak camera. With Ti targets unshifted $K\alpha$ predominates and the $K\alpha$ yield is observed to peak during the rising edge of the laser pulse. For aluminum targets the complete inner-shell transition spectrum extending up to the He-like resonance line is observed and is consistent with target heating expected from a local hot-electron flux comprising about 10% of the laser intensity during the rising slope of the pulse.

It is generally accepted that, at sufficiently high intensities, laser-target interaction is completely dominated by long mean-free-path electrons generated through resonance absorption and possibly other decay processes. At intensities in the range 10^{13}–10^{15} W/cm^2 with 10.6-μm lasers, direct absorption measurements[1,2] indicate that 30–40% of the incident laser energy is absorbed while x-ray continuum studies,[3–5] layered target $K\alpha$ calorimetry,[6,7] and fast-ion spectroscopy[8–10] indicate a primary heated electron distribution with $T_{\rm hot}\simeq 6\times10^{-5}\ (I\lambda^2)^{1/3}$ [(keV)/(W/cm^2 μm^2)$^{1/3}$]. The coupling of these long mean-free-path electrons into the dense target material is complicated in planar geometry by magnetic field supported lateral transport and fast-ion generation.[11–13] Direct measurements of local hot-electron energy deposition by $K\alpha$ calorimetry[7] and shock-wave velocity observations[14,15] indicate that about 10% of the laser energy is coupled into the target in the focal vicinity at target irradiances of 3×10^{14} W/cm^2. The dependence of yield on target depth in layered target $K\alpha$ experiments and the target thickness dependence of optically inferred rear surface temperature[7] are indicative of approximately classical axial transport of hot electrons at depths below 1 μm with a temperature scaling as described above.

$K\alpha$ flourescent yields from laser irradiated solid targets have been commonly used as a diagnostic of hot-electron or radiation-induced preheat in laser target interaction experiments.[16–18] In the case of hot-electron induced preheat an interpretation of these measurements has been handicapped by the absence of temporal resolution and a tendency for the unshifted or cold target $K\alpha$ emission to saturate at low absolute yields by preheat-induced target ionization.[16] This follows from the fact that, as outer electrons are removed by ionization, the energy of the inner shell vacancy transition increases because of reduced screening of the nuclear charge.[18] It has been suggested[19] that the observation of the complete spectrum of $K\alpha$ emission lines would thus serve as a direct diagnostic of ionization or temperature in dense target material.

In the present experiment we have combined a high-efficiency Von Hamos crystal spectrograph[20] with an x-ray streak camera. This has allowed for the first time the complete spectrum of $K\alpha$ emission lines from an Al target to be studied with temporal resolution. The results of these experiments using a 50-J, 1-nsec CO_2 laser to irradiate planar targets at an intensity of 3×10^{14} W/cm^2 are consistent with local hot-electron energy deposition during the rising portion of the laser pulse comprising $\sim$10% of the incident laser flux. Strong He-like resonance line emission is also observed from a thin (<500 Å) layer of Al near the target surface. This indicates energy deposition in the region immediately behind critical density, either through partial hot-electron transport inhibition or a thermal absorption process.

The experiment setup for these measurements is shown in Fig. 1. X rays were focused onto the slit of an x-ray streak camera by means of a 25×50 mm x-ray diffracting crystal bent to a 50-mm radius of curvature. The target and photocathode of the streak camera were located on the axis of curvature of the crystal with a separation of 300 mm. To record $K\alpha$ spectra from Al and Ti, x-ray diffracting crystals of RAP (rubidium acid phthalape) and PET (pentaerythritol) were used, respectively. The laser was incident in S polarization at an angle of 10° to the target normal allowing the photocathode to detect x-ray emission at 62.5° from target normal. The target consisted of a 75-μm-thick, 10×10-mm^2 foil mounted on a glass frame. For some shots the Al foil was covered with carbon film of thickness varying between 220 and 1000 Å.

The laser pulse had a rise time of 350–400 ps and a full width at half maximum of 750–900 ps. For the shots to be discussed here, the incident laser energy was in the range 40–50 J. The laser was focused onto the target by means of a 50-cm focal length $f/5$ plano-convex lens. The diameter of the focal spot at the first diffraction minimum was 125 μm with $\sim$50% of the incident laser energy contained within this diameter. The peak intensity at the center of the focal spot was in the range 3–4×10^{14} W/cm^2.

A typical time integrated spectrum of the x-ray emission from a pure Al target in the interval 7.7–8.4 Å is shown in Fig. 2(a) and a streak of the same spectral region is shown in Fig. 2(b). The positions of various $K\alpha$-like emission

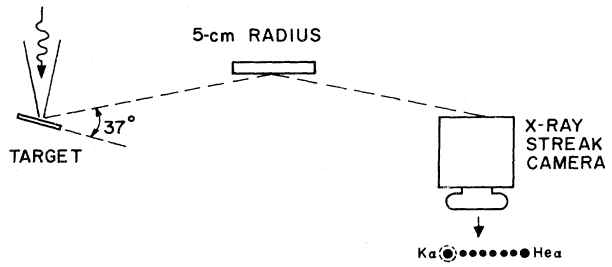

FIG. 1. Experimental setup for time-resolved x-ray streak spectra.

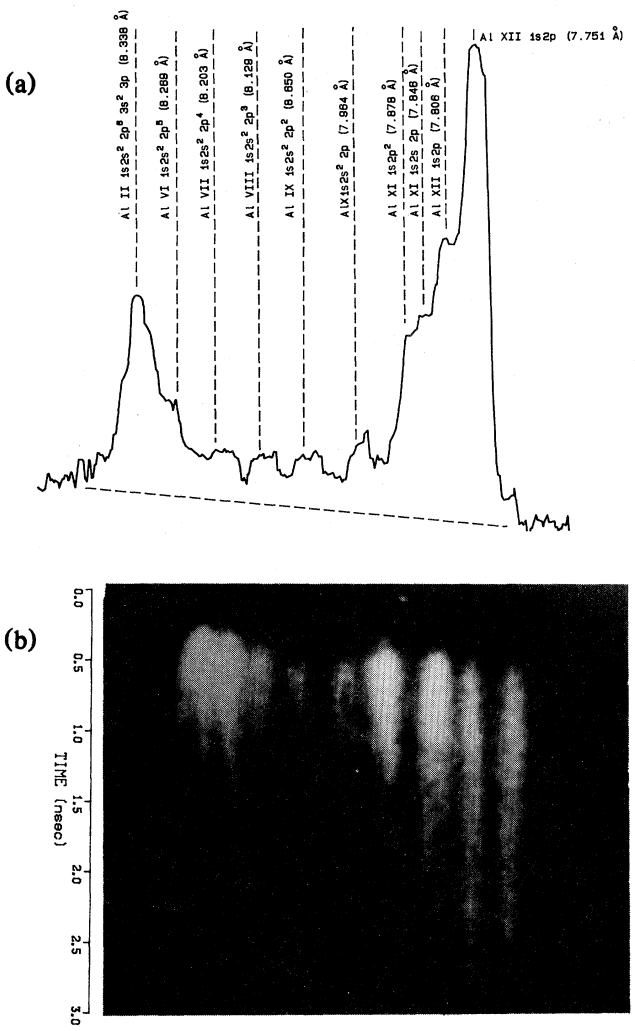

FIG. 2. (a) Typical time-integrated spectrum from Al target showing spectral region from cold $K\alpha$ (8.34 Å) to the He-like Al resonance line (7.76 Å). The intensity scale is approximately linear. (b) Streak photograph of same spectral region.

lines from the calculations of House[21] are included for comparison. It is apparent that emission bands corresponding to $K\alpha$ transitions resulting from inner-shell ionization of Al^{4+} to Al^{8+} are well resolved in both the time-integrated and streak photographs as well as the two emission lines from doubly excited Li-like aluminum (the so-called *j*, *k*, *l* and *q*, *r* satellite lines which can be populated by inner-shell ionization of excited Al^{9+}, inner-shell impact excitation of Al^{10+}, or dielectric recombination from Al^{11+}) and the He-like Al resonance and intercombination lines. $K\alpha$ emission from an expanding lateral transport zone which eventually extends several millimeters from the focal spot is indicated by an expanding ring of emission surrounding the cold $K\alpha$ line at 8.34 Å. This feature is similar to that previously reported in nonspectrally resolved x-ray streak photographs under similar conditions. The absence of this feature in $K\alpha$ emission lines from higher-ionization states is attributable to the low-specific energy deposition and consequent low degree of ionization in the lateral transport zone. The emission lines around 7.83 Å asssociated with the doubly excited Li-like configurations have previously been reported in laser target irradiation with 1-μm lasers[22] and have been explained in this case as due to transient ionization or dielectronic recombination of thermally produced Al^{11+}. In the present case, these lines actually appear slightly before resonance line emission. At a time $\sim$300 ps after the start of cold $K\alpha$ emission they are the most intense feature in the entire *K* shell transition spectrum. It seems likely, therefore, that in the present case these lines are a signature of inner-shell ionization by hot electrons of thermally produced Al^{9+} or inner-shell impact excitation of Al^{10+}.

In the case of pure Ti targets, Ti $K\alpha$ spectra recorded with a PET crystal exhibited only two weak-shifted $K\alpha$ components corresponding to Ti^{13+} and Ti^{14+}; the He-like Ti resonance line was not detected. The $K\alpha$ emission in the components Ti^{13+} and Ti^{14+} did not exceed a few percent of the total Ti $K\alpha$ yield.

The temporal dependences of cold $K\alpha$ emission (Al^{0+}–Al^{3+}), $K\alpha$ emission from Al^{7+}, and He-like Al resonance emission are shown in the photodensitometer traces of Figs. 3(a)–3(c) along with a typical laser pulse shape. The temporal dependence of $K\alpha$ emission from Ti is shown in Fig. 3(d). In this case since saturation by ionization is not important, the temporal dependence of $K\alpha$ emission should be proportional to the total rate of hot-electron energy deposition in the target. It can be seen from Fig. 3(d) that the duration of Ti $K\alpha$ emission is considerably less than the laser pulse length, and that if one associates the start of $K\alpha$ emission with the leading edge of the laser pulse, then this emission peaks on the rising edge of the pulse. In the case of Al targets, if one associates the start of the laser pulse with the initial appearance of cold $K\alpha$ emission, then this line peaks earlier than the Ti signal and its total duration is further shortened. The short duration of unshifted $K\alpha$ production in Al targets as compared with Ti is apparently indicative of thermal saturation of cold $K\alpha$ yield in Al. $K\alpha$ emission from Al^{7+} starts approximately 250 ps after cold $K\alpha$ emsission as does the He-like resonance emission. The long duration of the resonance line emission compared with the $K\alpha$ emission lines and the laser pulse width suggests that this line is primarily excited by thermal plasma.

Several spectra were obtained with overlays of carbon or plastic foil in the thickness range 200–1000 Å on the surface of an Al target foil. These spectra were qualitatively similar (with some attenuation) to those for pure Al, however, the He-like resonance line disappeared for overlays in excess of 500 Å. These observations suggest that a thin layer of target material is heated to a temperature in excess of 100 eV (this is consistent with the observation of weak Ti $K\alpha$ satellites corresponding to Ti^{13+} and Ti^{14+}). This heating occurs quite early in the laser pulse and is probably not associated with the main distribution of hot electrons responsible for $K\alpha$ production from deeper, cooler target layers. This may be due to partial hot-electron transport inhibition or simply a signature of weak thermal energy deposition at the critical density surface.

Target heating and hydrodynamic expansion under the influence of a hot-electron flux have been modeled by a version of the one-dimensional hydrocode MEDUSA.[23] The incidence laser pulse shape was modeled by a piecewise linear fit. At the critical density surface a constant fraction of the incident laser power was converted into an ingoing semi-isotropic flux of hot electrons at a temperature scaling with

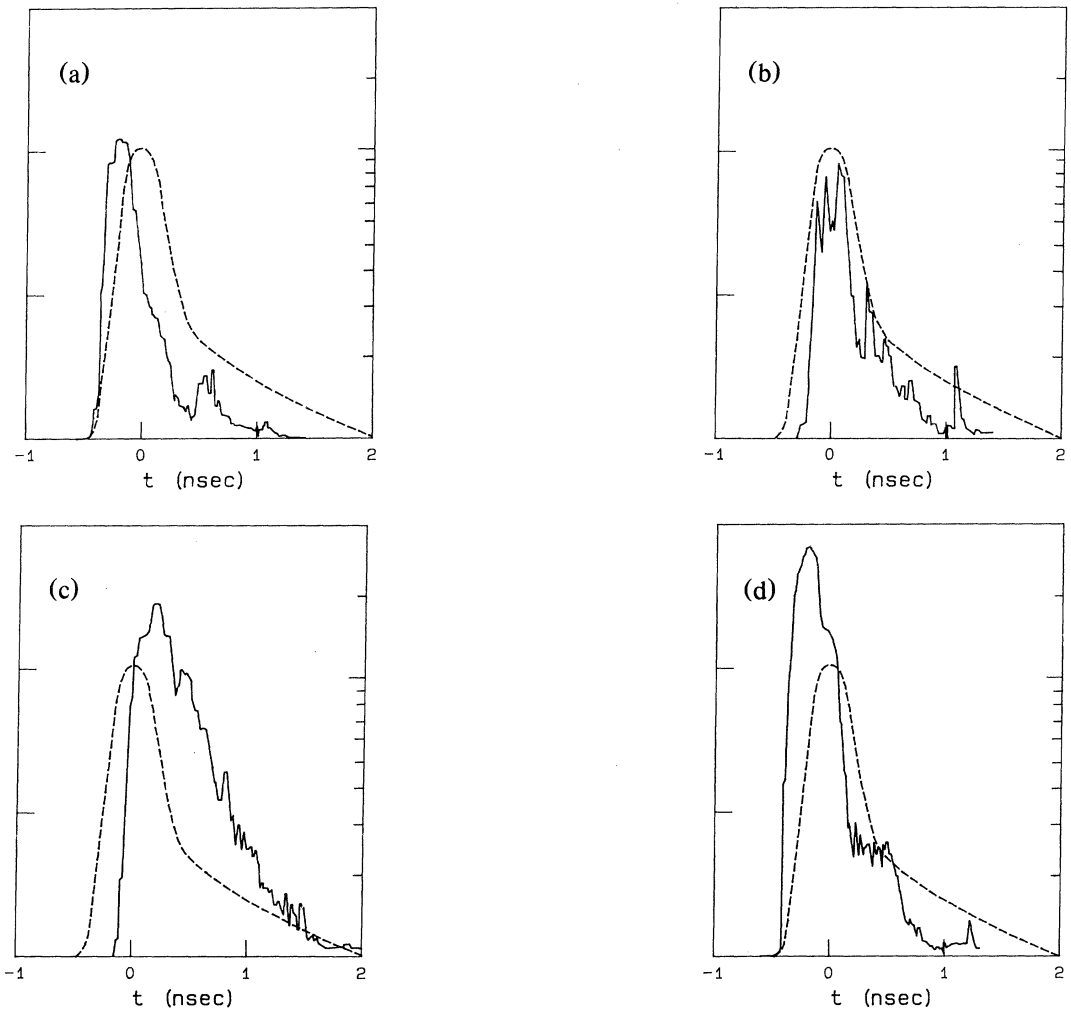

FIG. 3. Temporal characteristics of (a) cold Al $K\alpha$, (b) $K\alpha$ from Al^{7+}, (c) Al He-like resonance emission, and (d) Ti $K\alpha$ emission. The temporal profile of the laser pulse is in each case indicated by the dotted curve with assumption that cold $K\alpha$ emission starts at the leading edge of the laser pulse. Intensity scales are linear for laser intensity and logarithmic for the x-ray emission.

the incident laser intensity as $T_{\text{hot}} = 2.7 \times 10^{-4}\ I_1^{1/3}$ [keV/(W/cm^2)$^{1/3}$]. These electrons were assumed to deposit their energy in the dense target material according to the prescription of Harrach and Kidder.[24] The calculation used a Fermi-Thomas equation of state with Saha ionization. A temporally resolved spectrum of $K\alpha$ emission yields for various ionization states of Al was calculated by multiplying the rate of hot-electron energy deposition in each ionization state by the fluorescent yields calculated by McGuire.[19] This procedure assumes that the instantaneous ratio of energy deposited into K-shell ionizations to total electron energy deposition is independent of electron energy and ionization state. This approximation is reasonable providing that the hot-electron temperature is much greater than the K-shell ionization potential.[16] The lines were attenuated with target depth in an approximate fashion by taking an absorption coefficient corresponding to that of $K\alpha$ in cold Al and allowing for the experimentally correct angle of observation. The calculation thus ignores the possibility of $K\alpha$ absorption by resonant processes. Since MEDUSA calculates only an average degree of ionization, it was assumed that at most two ionization states were present in a given Lagrangian shell at one instant in time. The hot-electron flux at the surface of the target was assumed to be a constant fraction of the experimentally estimated peak laser intensity (that reached at the center of the focal spot). Calculated spectra for a laser pulse shape similar to the experimental one with a peak intensity of 3×10^{14} W/cm^2 are shown in Fig. 4 for assumed coupling fractions of 10% and 5%, respectively. It is apparent that the spectrum shown in Fig. 4(a) for a coupling fraction of 10% represents a reasonable fit to both the temporal behavior of the experimentally observed spectrum and the observed distribution of intensities among the various ionization states. For example, in the simulation Al^{7+} is produced 300 ps after the start of the laser pulse while, experimentally, the correpsonding $K\alpha$ line appears 250 ps after the onset of cold $K\alpha$. In the calculations the delay between the onset of emission from successively higher states is due to the time required for the zone of primary hot-electron energy deposition (extending 1–2 μm deep in the target at solid density) to reach the temperatures required for that degree of ionization. Ionization in the code is assumed to be instantaneously in thermal equilibrium. The appearance of Al^{7+}, for example, requires a thermal temperature of about 70 eV. At a given instant in time, emission from successively lower ionization states originates

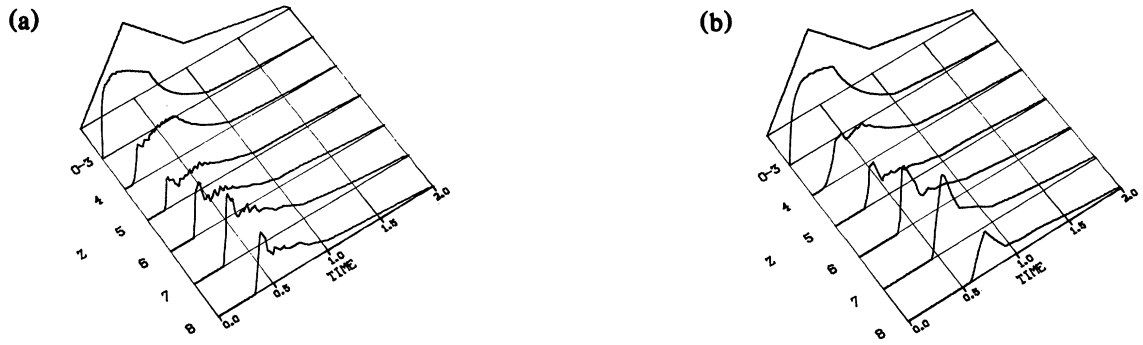

FIG. 4. Calculated distributions of $K\alpha$ yields in Al for (a) 10% coupling and (b) 5% coupling. The assumed laser pulse shape is indicated in each case by curve at upper left while descending curves represent yields from Al^{0-3+}, Al^{4+}, Al^{5+}, Al^{6+}, Al^{7+}, and Al^{8+}, respectively. The curves in (b) have been normalized so that the peak $K\alpha$ yield from cold Al (Al^{0-3+}) is equal in (a) and (b).

progressively deeper into the target. When the coupling efficiency is reduced from 10% to 5% in the simulation, the reduced rate of target heating is reflected in a larger delay between lines corresponding to higher charge states, Al^{8+}, for example, in this case is produced at the target surface only near the end of the laser pulse.

In addition to the strong dependence on target coupling efficiency, calculated $K\alpha$ emission spectra depend sensitively on details of hot-electron transport into the dense target material. Partial hot-electron transport inhibition near the target surface, for example, would result in an enhanced heating and ionization rate for a given coupling fraction. This will increase the relative strengths of $K\alpha$ emission from the higher ionization states. Although the present results are consistent with classical hot-electron transport and a coupling fraction of about 10% during the rising edge of the laser pulse, they do not rule out a reduced coupling fraction combined with axial hot-electron transport inhibition. The temporal dependence of unshifted $K\alpha$ production from Ti targets indicates that, in fact, the local hot-electron coupling efficiency varies with time during the laser pulse being greater on the rising edge.

As is evident from the calculations of Duston *et al.*,[19] $K\alpha$ radiation from Al targets can be produced by photon as well as electron energy deposition. In general, the relative contributions of photon- to electron-induced K-shell vacancies can be estimated by comparing the flux of photons escaping from the front of the target with energy above the K edge to the flux of hot electrons into the target, multiplied by their fractional energy dissipation in K-shell ionization[16] (about 2% for Al). An upper limit to the photon energy flux in the present case is about 5×10^{10} W/cm^2.[4] The hot-electron energy flux inferred from the present results and previous measurements is about 10% of the peak laser intensity or 3×10^{13} W/cm^2 giving a K-shell energy deposition of 6×10^{11} W/cm^2; thus the total contribution from x-ray induced inner-shell vacancies in the present case is at least an order of magnitude less than the contribution from hot-electron induced vacancies.

A careful study of the temporal evolution of shifted $K\alpha$ emission lines from layered low-Z targets should make it possible to directly infer target temperature as a function of depth and time thus resolving the temporal dependence of hot-electron coupling efficiency and establishing the exact nature of the transport of these electrons through the dense target material.

*Present address: Institut National de la Recherche Scientifique–Energie, Université du Québec, Varennes, Quebec J0L 2P0, Canada.

[1]D. M. Villeneuve, G. D. Enright, M. C. Richardson, and N. R. Isenor, J. Appl. Phys. 50, 3921 (1979).
[2]D. R. Bach *et al.*, Phys. Rev. Lett. 50, 2082 (1983).
[3]J. F. Kephart, R. P. Godwin, and G. H. McCall, Appl. Phys. Lett. 25, 108 (1974).
[4]G. D. Enright, N. H. Burnett, and M. C. Richardson, Appl. Phys. Lett. 31, 494 (1977).
[5]H. Pepin, F. Martin, B. Grek, T. W. Johnston, J. C. Kieffer, and C. Mitchel, J. Appl. Phys. 50, 6784 (1979).
[6]K. B. Mitchell and R. P. Godwin, J. Appl. Phys. 49, 3851 (1978).
[7]N. H. Burnett, N. A. Ebrahim, G. D. Enright, P. A. Jaanimagi, and C. Joshi, in Proceedings of the Japan–United States Seminar on Laser Produced Plasmas, Nara, 1982 (unpublished).
[8]A. W. Ehler *et al.*, J. Appl. Phys. 46, 2464 (1975).
[9]N. A. Ebrahim and C. Joshi, Phys. Fluids 24, 138 (1981).
[10]F. Begay and D. W. Forslund, Phys. Fluids 25, 1675 (1982).
[11]P. A. Jaanimagi, N. A. Ebrahim, N. H. Burnett, and C. Joshi, Appl. Phys. Lett. 38, 734 (1981).
[12]D. W. Forslund and J. V. Brackbill, Phys. Rev. Lett. 48, 1614 (1982).
[13]J. C. Kieffer, H. Pepin, M. Piche, J. P. Matte, T. W. Johnston, P. Lavigne, F. Martin, and R. Decoste, Phys. Rev. Lett. 50, 1054 (1983).
[14]P. D. Goldstone, R. F. Benjamin, and R. B. Schultz, Appl. Phys. Lett. 38, 223 (1981).
[15]N. H. Burnett, G. Josin, B. Ahlborn, and R. Evans, Appl. Phys. Lett. 38, 226 (1981).
[16]J. D. Hares, J. D. Kilkenney, M. H. Key, and J. G. Lunney, Phys. Rev. Lett. 42, 1216 (1979).
[17]B. Yaakobi, J. Deletrez, L. M. Goldman, R. L. McCrory, W. Seka, and J. M. Soures, Opt. Commun. 41, 355 (1982).
[18]A. Hauer, W. Priedhorsky, and D. van Hulsteyn, Appl. Opt. 20, 3477 (1981).
[19]D. Duston, R. W. Clark, J. Davis, and J. P. Apruzese, Phys. Rev. A 27, 1441 (1983).
[20]L. von Hamos, Z. Kristallogr. Kristallgeom. Kristallphys. Krystallchem. 101, 17 (1938).
[21]L. L. House, Astrophys. J. Suppl. Ser. 18, 21 (1969).
[22]U. Feldman, G. A. Doschek, D. J. Nagel, R. D. Cowan, and R. R. Whitlock, Astrophys. J. 192, 213 (1974).
[23]J. P. Christiansen, D. E. T. F. Ashbey, and K. V. Roberts, Comput. Phys. Commun. 7, 271 (1974).
[24]R. J. Harrach and R. E. Kidder, Phys. Rev. A 23, 887 (1981).

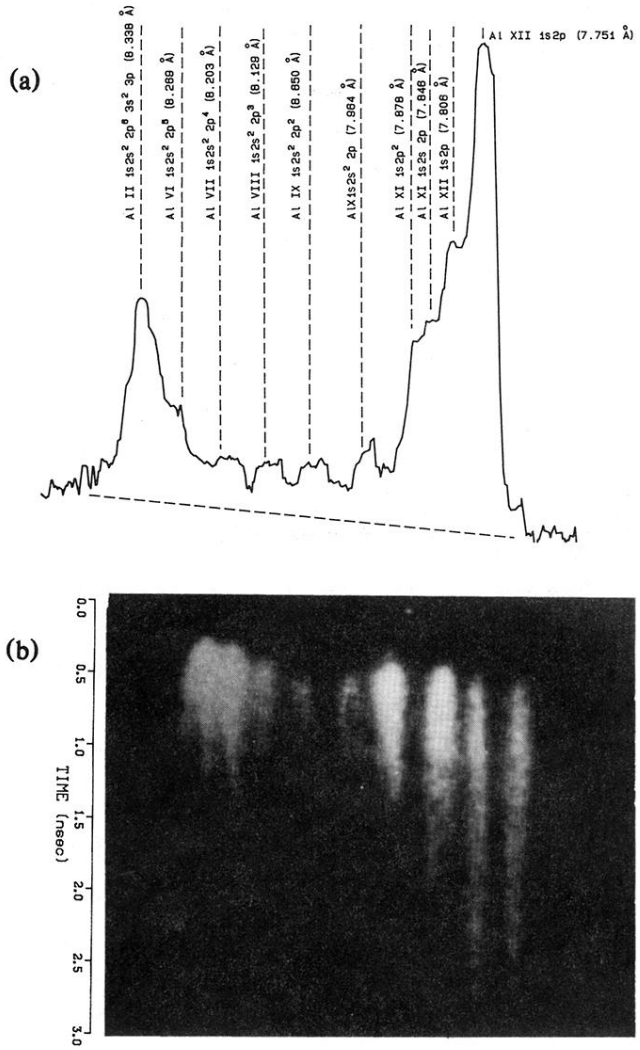

FIG. 2. (a) Typical time-integrated spectrum from Al target showing spectral region from cold $K\alpha$ (8.34 Å) to the He-like Al resonance line (7.76 Å). The intensity scale is approximately linear. (b) Streak photograph of same spectral region.